RSC Advances

PAPER

View Article Online
View Journal | View Issue

Cite this: *RSC Adv.*, 2021, **11**, 12614

An asymmetric Salamo-based Zn complex supported on Fe_3O_4 MNPs: a novel heterogeneous nanocatalyst for the silyl protection and deprotection of alcohols under mild conditions

Hongyan Yao,[a] Yongsheng Wang *[b] and Maryam Kargar Razi*[c]

In this study, a magnetic asymmetric Salamo-based Zn complex (H_2L = salen type di-Schiff bases)-supported on the surface of modified Fe_3O_4 (Fe_3O_4@H_2L-Zn) as a new catalyst was designed and characterized *via* numerous analytical techniques such as FT-IR spectroscopy, XRD, EDS, ICP-AES, SEM, TEM, TGA and VSM. An efficient and sustainable synthetic protocol has been presented for the synthesis of silyl ether substructures *via* the silyl protection of alcohols under mild conditions. The synthetic protocol involves a two-component solvent-free reaction between various hydroxyl-bearing substrates and hexamethyldisilazane (HMDS) as an inexpensive silylating agent using Fe_3O_4@H_2L-Zn MNPs as a magnetically separable, recyclable and reusable heterogeneous catalyst. Fe_3O_4@H_2L-Zn MNPs were also applied for the removal of silyl protecting groups from hydroxyl functions using water in CH_2Cl_2 under green conditions. The catalyst demonstrated good to excellent catalytic yield efficiency for both the reactions compared to the commercial metal-based catalysts under green conditions for a wide range of substrates.

Received 12th February 2021
Accepted 12th March 2021

DOI: 10.1039/d1ra01185e

rsc.li/rsc-advances

1. Introduction

In numerous preparation methods of delicate organic compounds, some specific parts of their molecules cannot survive the required reagents or chemical environments. Therefore, these parts, or groups, must be protected.[1–4] Regarding the number of protection and deprotection groups, it is highly significant to consider and reconsider the chemistry applied in unnatural structures and also in the building of nature's architecturally beautiful and diverse molecular frameworks. Usually attached to the asymmetrically substituted carbon atom, the hydroxyl group can be regarded as the most fundamental functional group in organic chemistry.[5–10] Therefore, it is evident that a wide variety of approaches have been disclosed and also the enantioselective synthesis of alcohols can be regarded as one of the most important steps in total synthesis.[11] Although there are important advances in the late-stage functionalization of complex molecules, the protection of hydroxyl groups is highly required during the succeeding steps.[12] In order to protect the alcohol group, there are several methods. In this sense, silylation can be regarded as one of the most common and easy methods in order to protect hydroxyl and thiol groups.[13] Silyl ethers are the most useful and important protecting groups for the protection of hydroxyl functional groups in organic chemistry from both synthetic and analytical point of views.[14]

During the recent decades, numerous types of silyl ethers have been developed *via* the reaction of silyl halides with parent alcohols in the presence of a base, such as triethylamine, pyridine, and *n*-butyl lithium.[15–17] To date, numerous procedures have been introduced for the silylation of alcohols using different silylation reagents in the presence of various catalysts including organo bases (*e.g.* *N*-oxides and *N*-halo reagents), iodine, trihalides, transition metals, Brønsted–Lowry acids as well as catalyst-free conditions.[2,18–20] These silylation methods are efficient, but unfortunately, they have serious disadvantages since they require a careful filtration or extraction process to remove the impurities derived from the reaction of by-product acids and co-bases during the silylation reaction.

Besides, R_3SiCl, MeSiN = C(Me)OSiMe, Me_3SiCl, or Me_3SiOTf in the presence of base are the reagents applied in the traditional and conventional processes.[12,21–29] Moreover, hexamethyldisilazane (HMDS) is a stable, commercially available and inexpensive reagent that can be used for the protection of hydroxy bearing compounds to trimethylsilyl ethers.[30–32] Its handling does not require special precautions, and the workup is not time-consuming because the by-product of the reaction is ammonia, which is easily removed from the reaction medium.[33,34]

[a]*Dean's Office, Hebi Polytechnic, Hebi 458030, China*
[b]*School of Physical Science Education, Henan Polytechnic University, Jiaozuo 454003, China. E-mail: yongshengw02@gmail.com; 454897487@qq.com; wys@hpu.edu.cn*
[c]*Faculty of Chemistry, North Branch of Tehran, Islamic Azad University, Tehran, Iran. E-mail: m_kargarrazi@iau-tnb.ac.ir*

The use of nanostructured heterogeneous catalysts in organic transformations has recently been very exciting owing to their catalytic efficiency and selectivity.[35–40] Furthermore, 2D materials have become an important platform to design numerous single-atom catalysts for diverse chemical reactions, such as N_2 reduction, CO_2 reduction, and CO oxidation.[41–52] The ease of isolation and separation of the heterogeneous catalysts from the desired organic product and the recyclability and reusability further enhanced the sustainability of the catalysts.[53–60] Moreover, the heterogeneous catalysts not only catalyze the reactions on their own, but also serve as an effective support for the immobilization of active catalysts and facilitate the efficient magnetic separation of the catalysts for their recovery and reusability.[61–63] The functionalization and modification of iron oxide nanoparticles with numerous biocompatible and biodegradable materials in many different ways have been demonstrated with efficient and effective catalysts.[59,64,65] Salen-based compounds can be considered as excellent candidates for the functionalization of iron oxide nanoparticles due to the presence of four coordination atoms (O, N, N, and O) in the center, which can coordinate with various metal ions to form M–Salen complexes.[66] The structure of metal ion coordination with nitrogen and oxygen of salen complexes has attracted considerable attention in the field of catalytic methods in organic syntheses due to their important and interesting variable structures, simple synthesis route, high efficiency with high selectivity and easy recycling of the catalysts.[67] Zinc is an inexpensive and readily available metal (zinc is easily extracted from the minerals in high purity). Low toxicity, low cost, abundance and accessibility of zinc make it attractive for application in catalysis chemistry.[68–71]

In the present study, we are concerned with the high yield synthesis of silyl ether substructures *via* the silyl protection of alcohols and phenols, followed by their deprotection *via* removal of silyl protecting groups from the hydroxyl functions under mild conditions using an asymmetric Salamo-based-Zn catalytic complex-functionalized magnetically separable nanocomposite as a recyclable and reusable nanocatalyst.

2. Experimental

2.1. Materials

All the reagents and solvents were purchased from Merck and used without additional purification.

2.2. Preparation of asymmetric Salamo-based-Zn supported on the surface of Fe_3O_4 MNPs

Fe_3O_4@APTES MNPs were prepared according to a previously reported method.[72] Then, its surface was functionalized by H_2L, which was prepared according to the procedure of Bian *et al.*[66] For the synthesis of asymmetric Salamo-based ligand supported on Fe_3O_4 nanoparticles, 1 g of the as-prepared Fe_3O_4@APTES was dispersed in 50 ml of toluene *via* sonication for 45 min, and then H_2L (3 mmol) was added to the mixture. The reaction

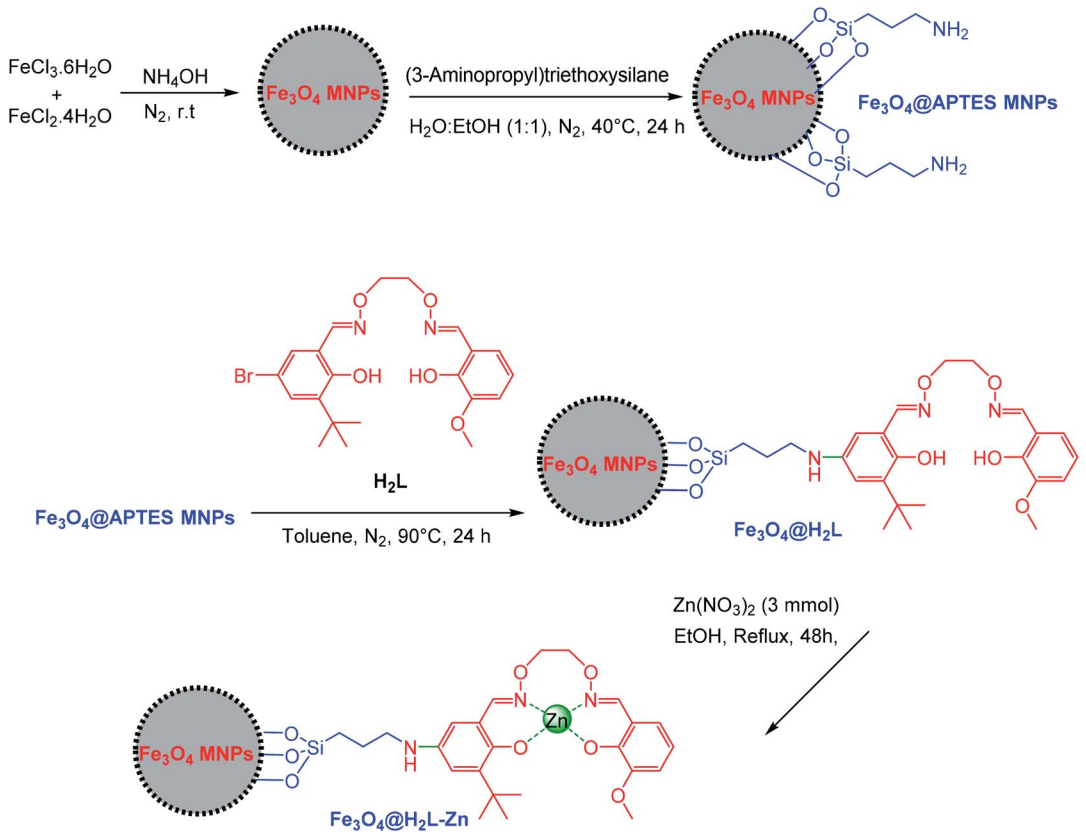

Scheme 1 The stepwise synthesis of Fe_3O_4@H_2L-Zn nanoparticles.

mixture was stirred under nitrogen atmosphere at reflux conditions for 24 h. Then, the obtained Fe_3O_4@H_2L product was separated *via* magnetic decantation and washed with hot ethanol and acetone to remove the unreacted ligand and dried in an oven at 50 °C for 8 h. The obtained Fe_3O_4@H_2L (0.5 g) was dispersed in 25 ml of ethanol by sonication for 60 min and then zinc nitrate (3 mmol) was added to the reaction mixture. The reaction mixture was stirred under nitrogen atmosphere at 80 °C for 48 h. The final product (Fe_3O_4@H_2L-Zn) was separated *via* magnetic filtration and washed with ethanol to remove the unattached substrates. The Fe_3O_4@H_2L-Zn nanoparticulate product was dried in an oven at 60 °C for 8 h (Scheme 1).

2.3. General procedure for the trimethylsilylation of alcohols

A mixture of alcohols (1 mmol), HMDS (0.8 mmol) and Fe_3O_4@H_2L-Zn (6 mg) was stirred at room temperature under solvent-free conditions and the progress of the reaction was monitored by TLC. After the completion of the reaction, the catalyst was separated by an external magnet and the mixture was decanted. Then, the mixture was washed with EtOAc and water to destroy the extra amounts of HMDS and organic layer was dried over anhydrous Na_2SO_4. The evaporation of the solvent under a reduced pressure obtain the pure product without further purification.

2.4. General procedure for the deprotection of silyl ether derivatives

Fe_3O_4@H_2L-Zn (6 mg) was added to a mixture of TMS ethers (1 mmol) in CH_2Cl_2 (4 ml) moistened by three drops of water and then the mixture was stirred at room temperature for the specified time and the progress of the reaction was monitored *via* TLC. After the completion of the reaction, the catalyst was separated by an external magnet and the mixture was decanted. The solvent was evaporated under a reduced pressure to obtain corresponding alcohols.

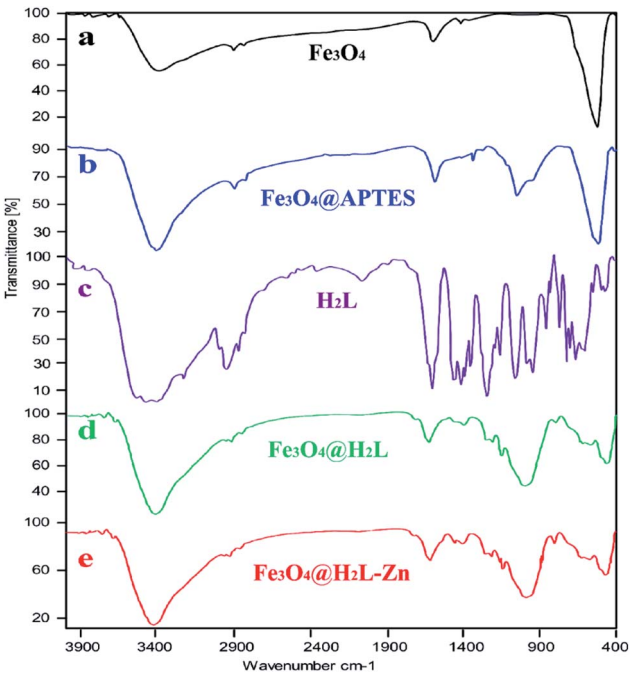

Fig. 1 FT-IR spectra of (a) Fe_3O_4, (b) Fe_3O_4@APTES, (c) H_2L, (d) Fe_3O_4@H_2L and (e) Fe_3O_4@H_2L-Zn MNPs.

3. Results and discussion

3.1. Synthesis and characterization of the catalyst

3.1.1. Design of catalyst. The magnetic nano catalyst was prepared based on Scheme 1. First, magnetic nanoparticles (Fe_3O_4) were synthesized according to the literature using $FeCl_3 \cdot 6H_2O$ and $FeCl_2 \cdot 4H_2O$ with the addition of NH_4OH.[72] In order to prevent the agglomeration of the nanoparticles during the synthesis, the Fe_3O_4 MNPs were dispersed and then (3-aminopropyl)triethoxysilane (APTES) was reacted with it until the amine functional group got attached to it. Next, an H_2L linker as the ligand was covalently bonded on the surface of Fe_3O_4@APTES groups by the intermolecular nucleophilic attack of the primary amine nucleophile to the haloalkane bond of H_2L. Finally, for the preparation of zinc-loaded materials, Fe_3O_4@H_2L-Zn particles were treated with $Zn(NO_3)_2$ as the Zn source (Scheme 1). The successful synthesis and physical and chemical properties of the as-prepared Fe_3O_4@H_2L-Zn was investigated *via* FT-IR spectroscopy, XRD, EDX, ICP-OEC, SEM, TGA and VSM techniques.

3.1.2. Chemical composition of the catalyst. The FT-IR spectra of the Fe_3O_4 (a), Fe_3O_4@APTES (b), H_2L (c), Fe_3O_4@h_2L (d) and Fe_3O_4@H_2L-Zn complex (e) are shown in Fig. 1. The FT-IR patterns in figure (a) and (b) are completely consistent with the previous analyses of Fe_3O_4 MNPs and Fe_3O_4@APTES, respectively.[72] In the FT-IR curves of H_2L and Fe_3O_4@H_2L (Fig. 1c and d), strong C=N stretching vibration band in the region of 1590–1615 cm^{-1}, C–O stretching vibration band around 1256 cm^{-1} and C=C band around 1456–1496 cm^{-1} provide evidences for the successful immobilization of the H_2L ligand on the surface of the modified support.[73] The shift on the C–O, C=N peaks in the Fe_3O_4@H_2L-Zn to more lower wavenumbers in comparison to the Fe_3O_4@H_2L confirm

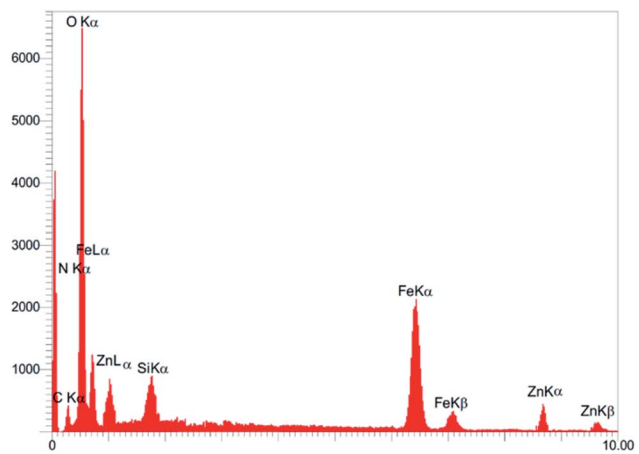

Fig. 2 EDX analysis of Fe_3O_4@H_2L-Zn MNPs.

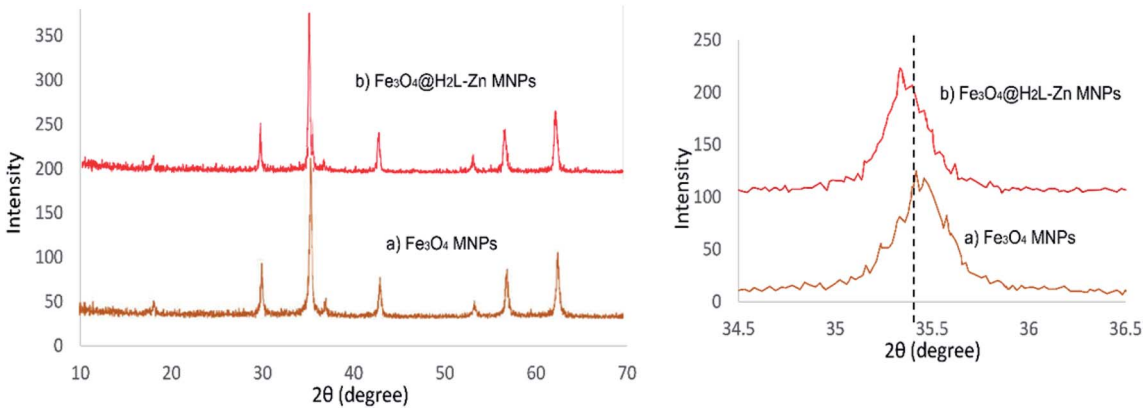

Fig. 3 XRD pattern of (a) Fe_3O_4 and (b) Fe_3O_4@H_2L-Zn MNPs.

the successful complexion of Zn ions with the oxime nitrogen atoms and phenol oxygen atoms.[73]

The presence of Fe, O, Si, C, N, and Pd elements on the surface of the catalyst were confirmed by energy dispersive X-ray (EDX) measurements and there were no other elements showing the high purity of the sample (Fig. 2). As shown in this Figure, the presence of N was observed but Br was not observed. This indicated that the covalent adsorption of the H_2L ligand successfully occurred on the catalyst surface. It is worth noting that the amount of zinc in Fe_3O_4@H_2L-Zn was 1.17×10^{-3} mol g^{-1}, which was determined by the ICP analysis.

Fig. 3 depicts the XRD patterns of Fe_3O_4 and Fe_3O_4@H_2L-Zn complex. In the Fe_3O_4 pattern, six major peaks were observed around $2\theta = 30°, 35°, 43°, 53°, 57°$, and $62°$ that corresponded to the (220), (311), (400), (422), (511), and (440) Miller indices, respectively. It can be seen in this figure that the Fe_3O_4@H_2L-Zn pattern is in good agreement with the characteristic peaks of bare Fe_3O_4, which indicates the retention of the crystalline spinel ferrite core structure during the functionalization of MNPs.[74] In the wide angle XRD pattern (Fig. 3b), the diffraction peaks corresponding to Zn ions cannot be observed for Fe_3O_4@H_2L-Zn, which reveals high zinc dispersion. The absence of Zn diffraction peaks indicates the formation of finely dispersed zinc species on the nanocomposite that are not detectable by this technique. However, the angles of the diffraction peaks of Fe_3O_4@H_2L-Zn decreased in comparsion to those of Fe_3O_4 nanoparticles, which confirm the presence of zinc ions in the final complex with high dispersion.[75]

3.1.3. Structure of the catalyst. Fig. 7 displays the FE-SEM images of Fe_3O_4@H_2L-Zn. These images illustrated the

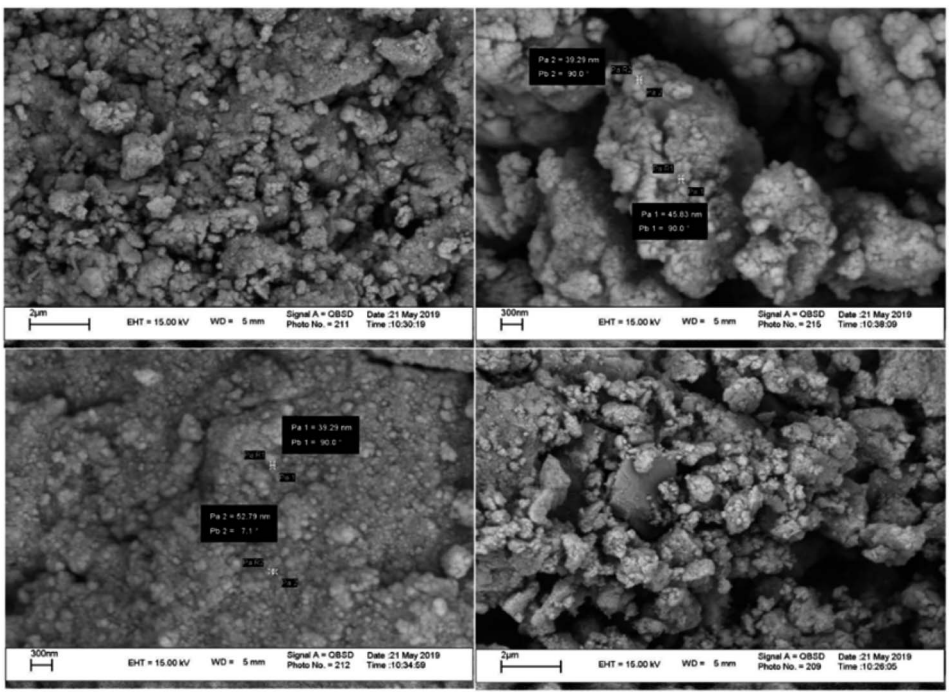

Fig. 4 SEM images of Fe_3O_4@H_2L-Zn MNPs.

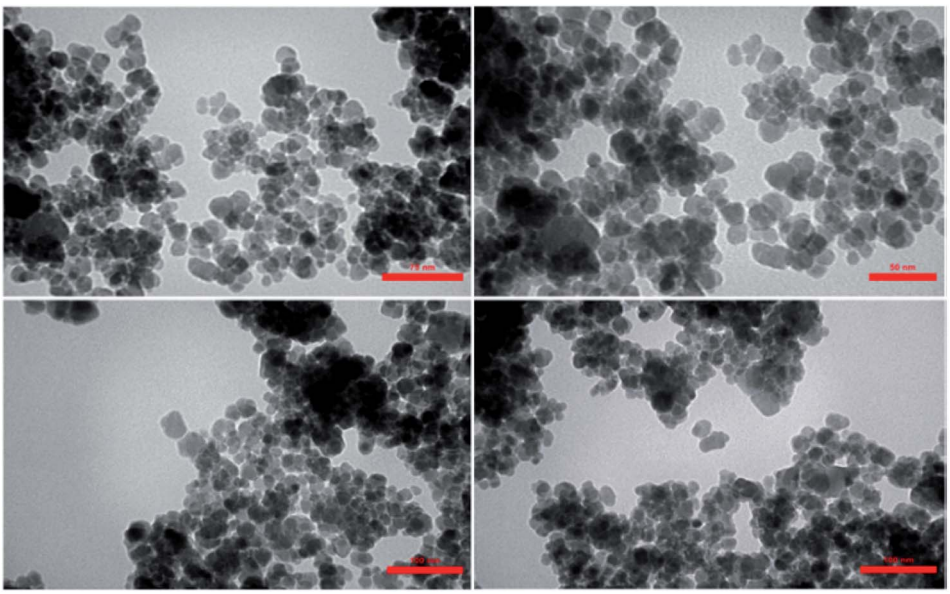

Fig. 5 TEM images of Fe_3O_4@H_2L-Zn MNPs.

presence of uniform and regular spherical particles. These type of particles are good candidates for both catalysis and adsorption processes (Fig. 4).

The morphology and average size of Fe_3O_4@H_2L-Zn were determined *via* transmission electron microscopy and the corresponding TEM micrographs are shown in Fig. 5. The TEM images show that the as-prepared nanocatalyst has almost a spherical-like shape with monodispersity. The average size of the as-synthesized Fe_3O_4@H_2L-Zn was 22 nm, with the maximum number of particles having size in the range of 18–21 nm.

3.1.4. Physicochemical properties of the catalyst. The thermal stability of Fe_3O_4, Fe_3O_4@APTES and Fe_3O_4@H_2L-Zn nanocomposites was examined by thermogravimetric analysis (TGA) (Fig. 6). In all of the TGA curves, the first obvious weight loss was found in the temperature range of 25–200 °C, which was attributed to the release of physically adsorbed moisture and solvent from the sample.[76] The other stage of gradual weight loss was found in the temperature range of 300–450 °C, which was caused by the decomposition of the APTES shells on the surface of the support. However, above 450 °C, catalyst decomposition started and the main weight change at 450–650 °C in the TGA curve represents the decomposition of the H_2L-Zn hybrid material.[77,78] As shown, the weight loss values of Fe_3O_4 to Fe_3O_4@H_2L-Zn MNPs increased sequentially. The results show that with the increase in temperature, the organic groups of the products are gradually decomposed in the process of pyrolysis, which confirms the successful chemical adsorption of the organic complex layers *via* chemical bonding on the modified Fe_3O_4 MNPs.

The vibrating sample magnetometer (VSM) technique was used to examine the magnetic properties of the Fe_3O_4@H_2L-Zn and its synthons. The saturation magnetization values of Fe_3O_4, Fe_3O_4@APTES, Fe_3O_4@H_2L, Fe_3O_4@H_2L-Zn and recovered Fe_3O_4@H_2L-Zn MNPs are shown in Fig. 7. As shown in the figure, the saturation magnetization (M_s) value from Fe_3O_4 to Fe_3O_4@H_2L-Zn decreased sequentially. This result confirms the

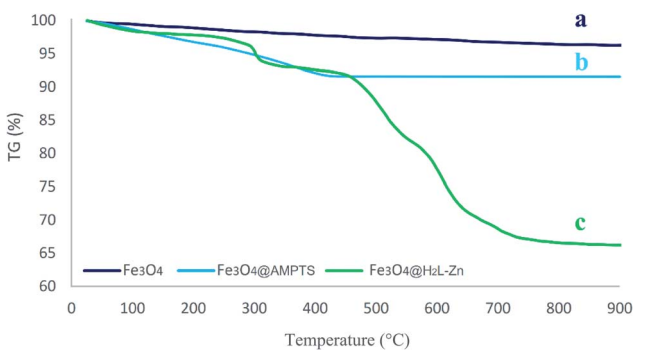

Fig. 6 TGA curve of Fe_3O_4, Fe_3O_4@APTES and Fe_3O_4@H_2L-Zn MNPs.

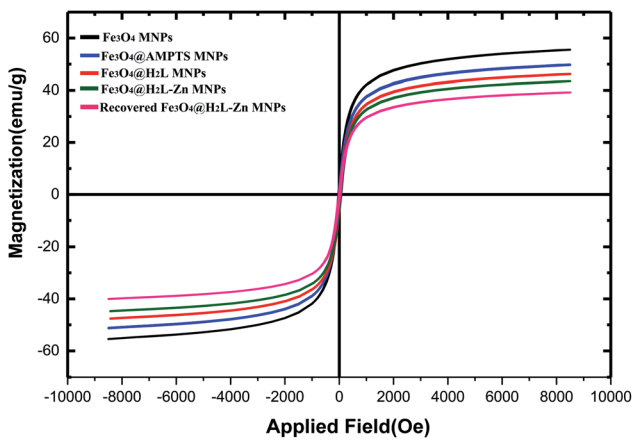

Fig. 7 VSM curves of Fe_3O_4, Fe_3O_4@APTES, Fe_3O_4@H_2L, $Fe_3O_4H_2$L-Zn and recovered Fe_3O_4@H_2L-Zn MNPs.

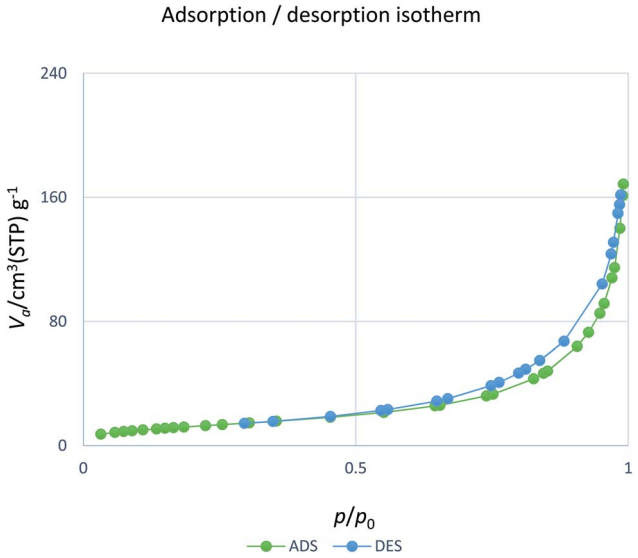

Fig. 8 Nitrogen adsorption/desorption isotherm of Fe_3O_4@H_2L-Zn MNPs.

successful chemical adsorption of the H_2L-Zn complex *via* chemical bonding with the modified Fe_3O_4 MNPs. As shown, the saturation magnetization value of Fe_3O_4@H_2L-Zn was 43 emu g^{-1}. Compared with that of Fe_3O_4 NPs (56 emu g^{-1}), this decrease can be attributed to the presence of H_2L-Zn and other functionalized groups on the surface of Fe_3O_4. The sequential decrease in the M_s value in each step can be a sufficient reason to confirm the successful immobilization of organic functional groups at different stages.

The nitrogen physisorption isotherm of the catalyst is shown in Fig. 8. The results of the BET analysis indicated that the highest surface area of the adsorbent was 121.92 m^2 g^{-1}. The large surface may endow the material with stronger catalytic activity. Furthermore, it can also be seen that the H_2L-Zn incorporation does not significantly change the BET parameters of the supports. This could indicate that the H_2L-Zn species are not incorporated into the framework but they are grafted on its surface.

3.2. Catalytic properties of the catalyst

After the successful synthesis and characterization of the Fe_3O_4@H_2L-Zn complex, we focused on its catalytic activity in the selective trimethylsilylation of alcohols as well as its catalytic activity in the deprotection of the as-prepared silyl ethers to parent alcohols.

For the optimization of reaction conditions, we studied the reaction of HMDS as a green silylation agent using benzyl alcohol in different conditions, and the effective reaction parameters including amount of the catalyst, type of solvent and temperature were optimized. The results show that the reaction promotion is highly affected by the catalyst loading and the solvent type. The effects of the catalyst amount in the reaction were examined by varying the catalyst loadings (2, 3, 4, 5, 6 and 7 mg) in the model reaction. It was observed that the yield of the trimethylsilyl ethers product enhanced with the increase in the amount of Fe_3O_4@H_2L-Zn from 2 to 6 mg (Table

Table 1 Optimization of the reaction conditions for the trimethylsilylation of benzyl alcohol (1 mmol) using HMDS (0.6 mmol) as a model compound

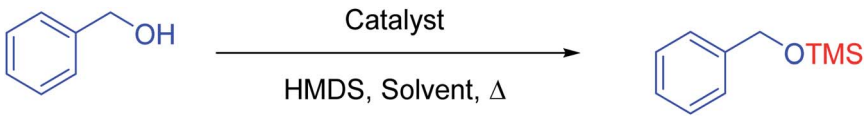

Entry	Catalyst	Catalyst (mg)	Solvent	Temperature	Time	Yield (%)
1	—	—	Solvent free	RT	12 h	NR
2	Fe_3O_4	6	Solvent free	RT	2 h	Trace
3	Fe_3O_4@APTES	6	Solvent free	RT	2 h	33
4	Fe_3O_4@H_2L	6	Solvent free	RT	2 h	Trace
5	Fe_3O_4@H_2L-Zn	2	Solvent free	RT	10	51
6	Fe_3O_4@H_2L-Zn	3	Solvent free	RT	10	83
7	Fe_3O_4@H_2L-Zn	4	Solvent free	RT	10	89
8	Fe_3O_4@H_2L-Zn	5	Solvent free	RT	10	96
9	Fe_3O_4@H_2L-Zn	6	Solvent free	RT	10	100
10	Fe_3O_4@H_2L-Zn	7	Solvent free	RT	10	100
11	Fe_3O_4@H_2L-Zn	6	Acetonitrile	RT	15	94
12	Fe_3O_4@H_2L-Zn	6	EtOAc	RT	20	95
13	Fe_3O_4@H_2L-Zn	6	*n*-Hexane	RT	15	92
14	Fe_3O_4@H_2L-Zn	6	THF	RT	10	97
15	Fe_3O_4@H_2L-Zn	6	CH_2Cl_2	RT	60	NR
16	Fe_3O_4@H_2L-Zn	6	Solvent free	45	7	100
17	Fe_3O_4@H_2L-Zn	6	Solvent free	60	5	100
18	Fe_3O_4@H_2L-Zn	6	Solvent free	90	5	100

Table 2 Catalytic trimethylsilylation of various alcohols with HMDS in the presence of 6 mg of Fe_3O_4@H_2L-Zn

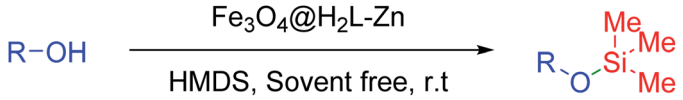

Entry	Substrate	Product	Time (min)	Yield[a,b] (%)
1	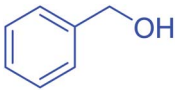	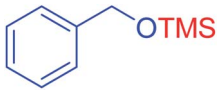	10	100
2	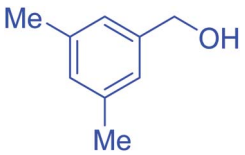	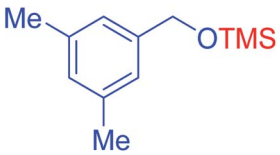	10	99
3	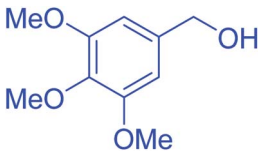	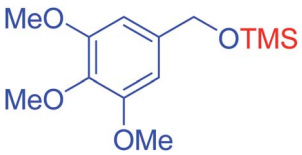	12	97
4	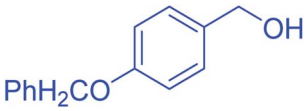	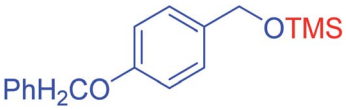	17	96
5	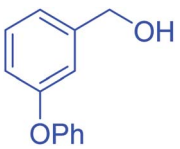	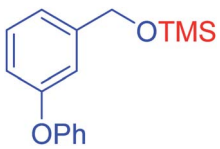	13	91
6	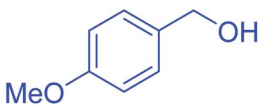	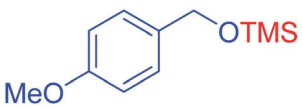	8	100
7	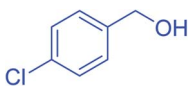	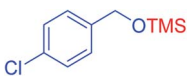	12	100
8	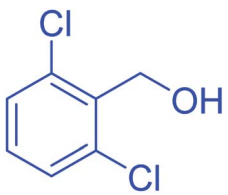	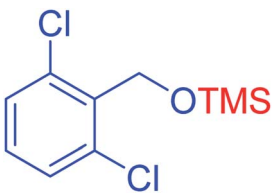	12	94
9	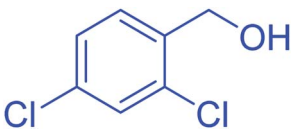	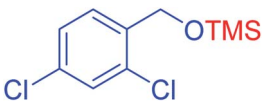	17	98
10	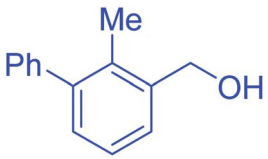	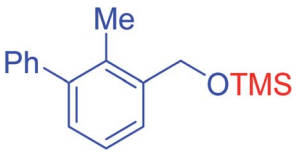	15	95
11	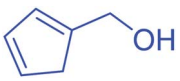	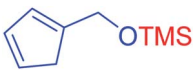	55	92

Table 2 (*Contd.*)

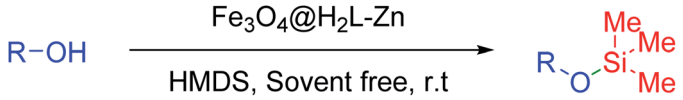

Entry	Substrate	Product	Time (min)	Yield[a,b] (%)
12	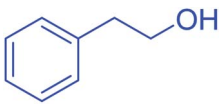	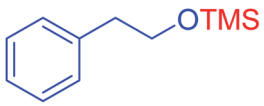	18	97
13	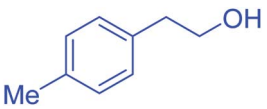	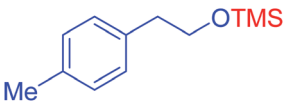	15	95
14	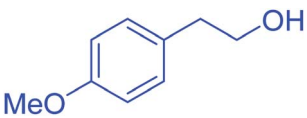	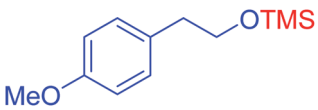	13	97
15	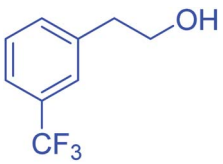	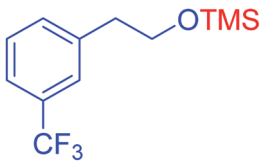	35	92
16	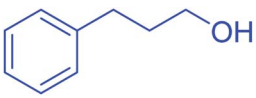	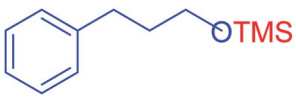	15	100
17	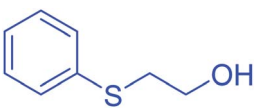	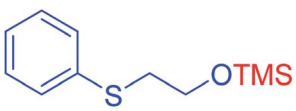	25	89
18	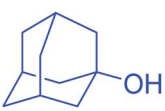	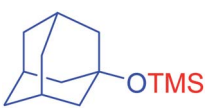	27	95
19	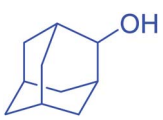	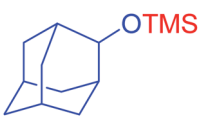	25	97
20	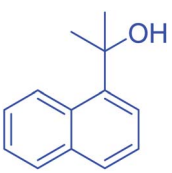	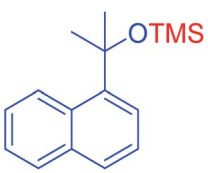	60	98
21	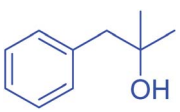	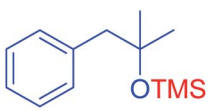	50	100
22			23	100

[a] Isolated yield. [b] Reaction conditions: alcohol (1 mmol), HMDS (0.8 mmol) and Fe_3O_4@H_2L-Zn (6 mg) at room temperature under solvent-free conditions.

1, entries 5–9). The best result in an appropriate time was obtained using 6 mg of the catalyst (Table 1, entry 9). It is worth mentioning that in the presence of 7 mg of Fe_3O_4@H_2L-Zn almost the same result as that in the presence of 6 mg was observed (Table 1, entry 10). Moreover, in the catalyst free conditions, the reaction did not proceed at all even after 12 h

(Table 1, entry 1). The efficiency of the catalyst was also considerably affected by the solvent (Table 1). Among the applied solvents such as acetonitrile, ethyl acetate, *n*-hexane, tetrahydrofuran, dichloromethane and solvent-free conditions, the best result was obtained in excellent yield after 10 min under solvent-free conditions as the reaction media (Table 1, entries 9 and 11–15). However, acetonitrile, ethyl acetate, *n*-hexane, tetrahydrofuran show good yields, but dichloromethane delivered a low yield of the corresponding product. By increasing the reaction temperature from 25 to 90 °C, the reaction time was reduced but room temperature was selected purely on the basis of green chemistry principle and high yield of the reaction in this condition. Finally, the best conditions for this coupling reaction are the following: Fe_3O_4@H_2L-Zn (6 mg), at room temperature under solvent-free conditions (Table 1, entry 9).

After the optimization of reaction conditions, the direct silylation of hydroxyl bearing compounds for the preparation of their corresponding trimethylsilyl ethers was studied under the obtained optimized reaction conditions. The results are presented in Table 2. As shown in Table 2, the Fe_3O_4@H_2L-Zn catalytic complex exhibited high efficiency in the solvent-free trimethylsilylation of numerous alcohols including several functional groups in excellent yields using hexamethyldisilazane under mild conditions at room temperature (25 °C). In this method, 24 different examples of benzylic and aliphatic alcohols including primary, bulky secondary, tertiary hydroxyl functional groups reacted with the HMDS (0.6 mmol) reagent and transformed to the corresponding trimethylsilyl ethers in good to excellent yields (89–100%) in short reaction time (8–60 min).

As silyl ether can be further converted to the parent alcohols under acidic conditions, the silylation of alcohols can be regarded as an alternative method for hydroxyl protection under ambient reaction conditions. Merging the silyl protection/deprotection of alcohols with modern methodologies, such as green chemistry and nanoscience, has added additional value to these temporary components of synthetic intermediates. Furthermore, in the final part of our studies, we report the use of the resulted nanocomposite (Fe_3O_4@H_2L-Zn) as a highly efficient catalyst for the chemoselective deprotection of some of the obtained trimethylsilyl ethers to their parent hydroxyl groups in wet dichloromethane moistened by 3 drops of water at room temperature. The results of this study are summarized in Table 3. As presented in Table 3, this catalytic system worked very well and the selected trimethylsilyl ethers gave the parent hydroxyl compounds in good to excellent yields in the presence of catalytic amount of (Fe_3O_4@H_2L-Zn) at room temperature.

Table 3 Deprotection of trimethylsilyl ethers (1 mmol) in the presence of the Fe_3O_4@H_2L-Zn catalyst in CH_2Cl_2 (4 ml) moistened by 3 drops of water at room temperature

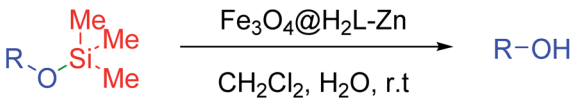

Entry	Substrate	Product	Time (min)	Yield[a,b](%)
1	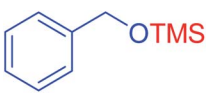	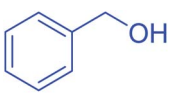	15	100
2	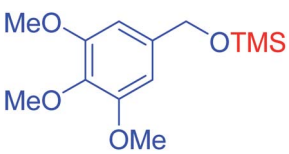	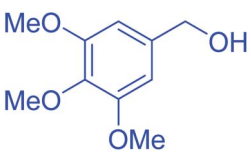	23	100
3	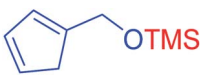	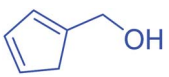	85	98
4	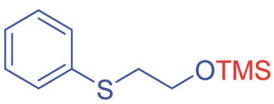	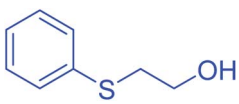	37	96
5	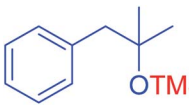	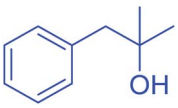	47	100
6			29	100

[a] Isolated yield. [b] Reaction conditions: TMS ethers (1 mmol), HMDS (0.8 mmol) and Fe_3O_4@H_2-Zn (6 mg) at room temperature in CH_2Cl_2 (4 ml) moistened by three drops of water.

Table 4 Comparing catalytic activity of Fe_3O_4@H_2L-Zn with previously reported methods in the trimethylsilylation of benzyl alcohol

Entry	Catalyst	Time (min)	Yield[a] (%)	Ref.
1	$La(NO_3)_3 \cdot 6H_2O$	95	98	79
2	Au/TiO_2	60	96	80
3	Natural kaolinitic clay	120	91	81
4	Aliquat 336	240	82	82
5	Fe_3O_4@H_2L-Zn	10	100	This work

[a] Isolated yield.

3.3. Scale-up production

Developing a strategy for scaling up of the protection and deprotection of alcohols is a challenge for numerous drug and pharmaceutical manufacturers. Attempting larger-scale chemical fabrication with reactions previously optimized at the laboratory scale is a big challenge. To clearly demonstrate the potential of this method for the scaled up protection of benzyl alcohol and deprotection of its corresponding trimethylsilyl ether to its parent hydroxyl compound, the reactions were investigated using 20.0 mmol of substrates under optimized conditions. Desired protected and deprotected products were obtained in 97 and 95% yields, respectively.

4. Recycling ability, hot filtration and leaching tests of the catalyst

Recyclability is one of the most important properties of heterogeneous catalysts. The recyclability of the catalyst Fe_3O_4@H_2L-Zn was studied in a typical trimethylsilylation reaction with benzyl alcohol and HMDS under the optimized reaction conditions. Briefly, after the finalization of each run of the trimethylsilylation reaction, which was monitored by TLC, the heterogeneous catalyst was separated using an external magnet, washed with acetone and water and dried overnight under vacuum at 60 °C to use in the next run. Fig. 9 shows that the Fe_3O_4@H_2L-Zn complex can be reused 10 times and the catalytic activity was not significantly reduced and it was indicated that the catalyst has good recyclability. It was also proved by the hot filtration test that the Fe_3O_4@H_2L-Zn complex played a catalytic role in the reaction rather than the free Zn in the solution. Furthermore, difference in the Zn content for the fresh and reused catalyst, after eight run, was only 0.5%, proving a low rate of leaching.

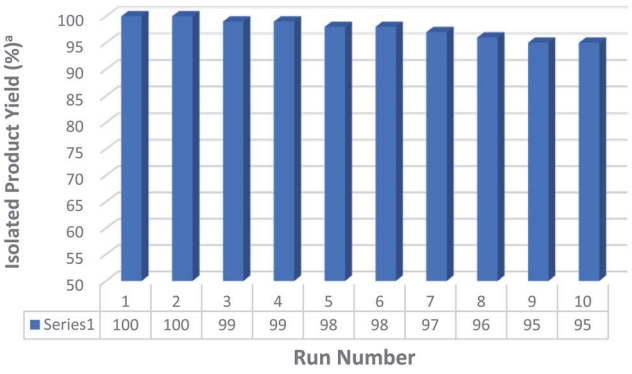

Fig. 9 Recyclability of the catalyst.

5. Comparison

In order to investigate the efficiency of this new procedure compared to the reported procedures in the literature, the results for the trimethylsilylation of benzyl alcohol as the representative example was compared to the best of the well-known data from the literature, as outlined in Table 4. The comparison results show that the present catalytic system modified the Heck reaction time, yields and conditions.

6. Conclusion

In summary, a novel catalyst H_2L-Zn complex was successfully prepared on the Fe_3O_4 surface and was characterized by a progressive mode for the preparation. The Fe_3O_4@H_2L-Zn catalysts have an efficient catalytic activity for the silyl protection and deprotection of alcohols by the selective trimethylsilylation of primary, secondary and tertiary aromatic and aliphatic alcohols in high yields in green media at 25 °C in low reaction times. More importantly, Fe_3O_4@H_2L-Zn has several advantages such as simple to synthesize, wide range of carriers, ligand-free protocol and easy to separate the use of commercially available, eco-friendly, inexpensive and chemically stable reagents with operational simplicity, practicability and good to high yields. The separation of products and recycling of catalysts are easier and simpler with the assistance of an external magnet. The catalyst can be reused 10 times with little loss of activity.

7. Data availability

The data that support the findings of this study are available from the corresponding author upon reasonable request.

Conflicts of interest

There are no conflicts to declare.

References

1 M. Mohebbi, P. Salehi, M. Bararjanian and S. N. Ebrahimi, *J. Iran. Chem. Soc.*, 2018, **15**, 47–53.
2 Y. Horino, M. Ishibashi, K. Nakasai and T. Korenaga, *Tetrahedron*, 2020, **76**, 131493.
3 Y. Yang, M. Lin, J. Tang, S. Ma and Y. Yu, *Anal. Bioanal. Chem.*, 2020, **412**, 6679–6690.
4 J. Grzybek, M. Kubů, W. J. Roth, B. Gil, J. Čejka and V. Kasneryk, *Catal. Today*, 2020, **354**, 133–140.
5 E. Indarti, H. Marwan, R. Rohaizu and W. D. Wanrosli, *Int. J. Biol. Macromol.*, 2019, **135**, 106–112.

6 J. F. Hartwig and E. A. Romero, *Tetrahedron*, 2019, **75**, 4059–4070.
7 J. Seliger and M. Oestreich, *Chem.–Eur. J.*, 2019, **25**, 9358–9365.
8 S. Sittihan and T. F. Jamison, *J. Am. Chem. Soc.*, 2019, **141**, 11239–11244.
9 Y. Liu, Q. Zhang, M. Xu, H. Yuan, Y. Chen, J. Zhang, K. Luo, J. Zhang and B. You, *Appl. Surf. Sci.*, 2019, **476**, 632–640.
10 C. Zuo, Q. Chen, L. Tian, L. Waller and A. Asundi, *Opt. Lasers Eng.*, 2015, **71**, 20–32.
11 R. Das and D. Chakraborty, *Appl. Organomet. Chem.*, 2012, **26**, 140–144.
12 M. Mittersteiner, M. A. Voigt, P. C. de Jesus and P. B. Brondani, *ChemistrySelect*, 2018, **3**, 10717–10720.
13 K. Yoshida and K. I. Takao, *Tetrahedron Lett.*, 2014, **55**, 6861–6863.
14 J. Seliger, X. Dong and M. Oestreich, *Angew. Chem., Int. Ed.*, 2019, **58**, 1970–1974.
15 S. Yoshimatsu and K. Nakata, *Adv. Synth. Catal.*, 2019, **361**, 4679–4684.
16 K. Hyodo, S. Gandhi, M. Van Gemmeren and B. List, *Synlett*, 2015, **26**, 1093–1095.
17 T. Avullala, P. Asgari, Y. Hua, A. Bokka, S. G. Ridlen, K. Yum, H. V. R. Dias and J. Jeon, *ACS Catal.*, 2019, **9**, 402–408.
18 M. Marin-Luna, B. Pölloth, F. Zott and H. Zipse, *Chem. Sci.*, 2018, **9**, 6509–6515.
19 B. F. Bergel, L. Leite Araujo, A. L. dos Santos da Silva and R. M. Campomanes Santana, *Carbohydr. Polym.*, 2020, **241**, 116274.
20 T. Nagy, Á. Kuki, L. Nagy, M. Zsuga and S. Kéki, *J. Mass Spectrom.*, 2018, **53**, 240–246.
21 X. Wang, P. Li, Z. Li, W. Chen, H. Zhou, Y. Zhao, X. Wang, L. Zheng, J. Dong, Y. Lin, X. Zheng, W. Yan, J. Yang, Z. Yang, Y. Qu, T. Yuan, Y. Wu and Y. Li, *Chem. Commun.*, 2019, **55**, 6563–6566.
22 P. Bunse, C. Schlepphorst, F. Glorius, M. Kitamura and B. Wünsch, *J. Org. Chem.*, 2019, **84**, 13744–13754.
23 J. E. Radcliffe, V. Fasano, R. W. Adams, P. You and M. J. Ingleson, *Chem. Sci.*, 2019, **10**, 1434–1441.
24 C. Llorente, R. Jimenez, J. Jackie, Y. Brotman, A. R. Fernie and N. Sreenivasulu, *Methods Mol. Biol.*, 2019, **1892**, 187–199.
25 R. Hrdina, *Synthesis*, 2019, **51**, 629–642.
26 B. Su, T. Lee and J. F. Hartwig, *J. Am. Chem. Soc.*, 2018, **140**, 18032–18038.
27 D. I. Zhilyaev, L. G. Voskresensky, N. Y. Polovkov and R. S. Borisov, *J. Anal. Chem.*, 2018, **73**, 1323–1326.
28 C. Díez-Poza, P. Val, F. Pulido and A. Barbero, *Mar. Drugs*, 2018, **16**, 421.
29 S. De Pooter, S. Latré, F. Desplentere and D. Seveno, *J. Non-Cryst. Solids*, 2018, **499**, 217–226.
30 M. Galehassadi and S. Pourreza, *J. Inorg. Organomet. Polym. Mater.*, 2019, **29**, 541–549.
31 N. Anbu, C. Vijayan and A. Dhakshinamoorthy, *Mol. Catal.*, 2019, **474**, 110357.
32 A. Azad, M. G. Dekamin, S. Afshar, A. Tadjarodi and A. Mollahosseini, *Res. Chem. Intermed.*, 2018, **44**, 2951–2963.
33 M. Yadegari, M. Moghadam, S. Tangestaninejad, V. Mirkhani and I. Mohammadpoor-Baltork, *Polyhedron*, 2012, **31**, 332–338.
34 S. T. Kadam and S. S. Kim, *Green Chem.*, 2010, **12**, 94–98.
35 Z. Zhuang and D. Liu, *Nano-Micro Lett.*, 2020, **12**, 132.
36 C. Megías-Sayago, S. Navarro-Jaén, R. Castillo and S. Ivanova, *Curr. Opin. Green Sustain. Chem.*, 2020, **21**, 50–55.
37 N. Kaur, N. Ahlawat, P. Bhardwaj, Y. Verma, P. Grewal and N. K. Jangid, *Synth. Commun.*, 2020, **50**, 137–160.
38 X. Wang, J. Wang, X. Sun, S. Wei, L. Cui, W. Yang and J. Liu, *Nano Res.*, 2018, **11**, 988–996.
39 X. Li, R. Zhang, X. Zhang, P. Zhu and T. Yao, *Chem.–Asian J.*, 2020, **15**, 1175–1179.
40 Y. Liu, B. Hu, S. Wu, M. Wang, Z. Zhang, B. Cui, L. He and M. Du, *Appl. Catal., B*, 2019, **258**, 117970.
41 C.-X. Huang, G. Li, L.-M. Yang and E. Ganz, *ACS Appl. Mater. Interfaces*, 2021, **13**, 608–621.
42 B. Song, Y. Zhou, H.-M. Yang, J.-H. Liao, L.-M. Yang, X.-B. Yang and E. Ganz, *J. Am. Chem. Soc.*, 2019, **141**, 3630–3640.
43 L. Xu, L.-M. Yang and E. Ganz, *Theor. Chem. Acc.*, 2018, **137**, 98.
44 Y. Liu, L.-M. Yang and E. Ganz, *Condens. Matter*, 2019, **4**, 65.
45 J. Yang, X. Wang, Y. Qu, X. Wang, H. Huo, Q. Fan, J. Wang, L.-M. Yang and Y. Wu, *Adv. Energy Mater.*, 2020, **10**, 2001709.
46 L.-M. Yang, V. Bačić, I. A. Popov, A. I. Boldyrev, T. Heine, T. Frauenheim and E. Ganz, *J. Am. Chem. Soc.*, 2015, **137**, 2757–2762.
47 J.-H. Liu, L.-M. Yang and E. Ganz, *ACS Sustainable Chem. Eng.*, 2018, **6**, 15494–15502.
48 J.-H. Liu, L.-M. Yang and E. Ganz, *J. Mater. Chem. A*, 2019, **7**, 3805–3814.
49 J.-H. Liu, L.-M. Yang and E. Ganz, *J. Mater. Chem. A*, 2019, **7**, 11944–11952.
50 J.-H. Liu, L.-M. Yang and E. Ganz, *RSC Adv.*, 2019, **9**, 27710–27719.
51 J.-H. Liu, L.-M. Yang and E. Ganz, *Energy Environ. Mater.*, 2019, **2**, 193–200.
52 R. Tong, Z. Sun, X. Wang, L. Yang, J. Zhai, S. Wang and H. Pan, *Int. J. Hydrogen Energy*, 2020, **45**, 18912–18921.
53 S. Kumar, S. Jain, M. Nehra, N. Dilbaghi, G. Marrazza and K.-H. Kim, *Coord. Chem. Rev.*, 2020, **420**, 213407.
54 M. Ghabdian, M. A. Nasseri, A. Allahresani and A. Motavallizadehkakhky, *Appl. Organomet. Chem.*, 2018, **32**, e4545.
55 Q. Jia, S. Huang, M. Hu, Y. Song, M. Wang, Z. Zhang and L. He, *Sens. Actuators, B*, 2020, **323**, 128647.
56 X. Li, Y. Feng, B. Liu, D. Yi, X. Yang, W. Zhang, G. Chen, Y. Liu and P. Bai, *J. Alloys Compd.*, 2019, **788**, 485–494.
57 Y. Song, M. Xu, Z. Li, L. He, M. Hu, L. He, Z. Zhang and M. Du, *Sens. Actuators, B*, 2020, **321**, 128527.
58 P. Xu, W. Lu, J. Zhang and L. Zhang, *ACS Sustainable Chem. Eng.*, 2020, **8**, 12366–12377.
59 M. Shi, B. Wang, Y. Shen, J. Jiang, W. Zhu, Y. Su, M. Narayanasamy, S. Angaiah, C. Yan and Q. Peng, *Chem. Eng. J.*, 2020, **399**, 125627.
60 A. Kazemi and S. Yang, *JOM*, 2019, **71**, 1209–1214.

61 M. Wang, M. Hu, Z. Li, L. He, Y. Song, Q. Jia, Z. Zhang and M. Du, *Biosens. Bioelectron.*, 2019, **142**, 111536.
62 Z. Lei, S. Hao, J. Yang, L. Zhang, B. Fang, K. Wei, Q. Lingbo, S. Jin and C. Wei, *Chemosphere*, 2021, **270**, 128646.
63 Y.-C. Wang, K. Huang, X. Lai, Z. Shi, J.-B. Liu and G. Qiu, *Org. Biomol. Chem.*, 2021, **19**(9), 1940–1944.
64 R. Hudson, Y. Feng, R. S. Varma and A. Moores, *Green Chem.*, 2014, **16**, 4493–4505.
65 M. Wang, L. Yang, B. Hu, J. Liu, L. He, Q. Jia, Y. Song and Z. Zhang, *Biosens. Bioelectron.*, 2018, **113**, 16–24.
66 R.-N. Bian, J.-F. Wang, X. Xu, X.-Y. Dong and Y.-J. Ding, *Appl. Organomet. Chem.*, 2020, e6040.
67 T. Rasheed, A. A. Hassan, M. Bilal, T. Hussain and K. Rizwan, *Chemosphere*, 2020, **259**, 127369.
68 C. J. Rhodes, *Sci. Prog.*, 2010, **93**, 223–284.
69 H. J. Yoo and S. W. Youn, *Org. Lett.*, 2019, **21**, 3422–3426.
70 M. A. Wani, A. Kumar, M. D. Pandey and R. Pandey, *Polyhedron*, 2017, **126**, 142–149.
71 X. Pan, Z. Liu, R. Cheng, X. He and B. Liu, *J. Organomet. Chem.*, 2015, **775**, 67–75.
72 U. Kurtan and A. Baykal, *Mater. Res. Bull.*, 2014, **60**, 79–87.
73 M. Asadi, K. Mohammadi, S. Esmaielzadeh, B. Etemadi and H. K. Fun, *Polyhedron*, 2009, **28**, 1409–1418.
74 V. A. J. Silva, P. L. Andrade, M. P. C. Silva, D. A. Bustamante, L. De Los Santos Valladares and J. Albino Aguiar, *J. Magn. Magn. Mater.*, 2013, **343**, 138–143.
75 Z. Lv, Q. Wang, Y. Bin, L. Huang, R. Zhang, P. Zhang and M. Matsuo, *J. Phys. Chem. C*, 2015, **119**, 26128–26142.
76 B. Maleki, O. Reiser, E. Esmaeilnezhad and H. J. Choi, *Polyhedron*, 2019, **162**, 129–141.
77 L. Moradi and M. Tadayon, *J. Saudi Chem. Soc.*, 2018, **22**, 66–75.
78 A. Ahmadi, T. Sedaghat, R. Azadi and H. Motamedi, *Catal. Lett.*, 2020, **150**, 112–126.
79 B. Akhlaghinia, *Phosphorus, Sulfur Silicon Relat. Elem.*, 2009, **184**, 2530–2535.
80 C. Gryparis and M. Stratakis, *Chem. Commun.*, 2012, **48**, 10751.
81 T. T. Upadhya, T. Daniel, A. Sudalai, T. Ravindranathan and K. R. Sabu, *Synth. Commun.*, 1996, **26**, 4539–4544.
82 M. Lissel and J. Weiffen, *Synth. Commun.*, 1981, **11**, 545–549.